



HAL
open science

Calibration of thermo-viscoplastic constitutive model under biaxial loadings: A Feasibility Study

Zhihao Wang, Dominique Guines, Lionel Leotoing

► **To cite this version:**

Zhihao Wang, Dominique Guines, Lionel Leotoing. Calibration of thermo-viscoplastic constitutive model under biaxial loadings: A Feasibility Study. International ESAFORM Conference 2023, Apr 2023, Krakow, Poland. pp.1397-1406, 10.21741/9781644902479-151 . hal-04093006

HAL Id: hal-04093006

<https://hal.science/hal-04093006>

Submitted on 16 May 2023

HAL is a multi-disciplinary open access archive for the deposit and dissemination of scientific research documents, whether they are published or not. The documents may come from teaching and research institutions in France or abroad, or from public or private research centers.

L'archive ouverte pluridisciplinaire **HAL**, est destinée au dépôt et à la diffusion de documents scientifiques de niveau recherche, publiés ou non, émanant des établissements d'enseignement et de recherche français ou étrangers, des laboratoires publics ou privés.



Distributed under a Creative Commons Attribution 4.0 International License

Calibration of thermo-viscoplastic constitutive model under biaxial loadings: A Feasibility Study

WANG Zhihao^{1,a}, GUINES Dominique^{1,b} and LEOTOING Lionel^{1,c*}

¹ Univ Rennes, INSA Rennes, LGCGM (Laboratoire de Génie Civil et Génie Mécanique), F-35000 Rennes, France

^azhihao.wang@insa-rennes.fr, ^bdominique.guines@insa-rennes.fr,

^clionel.leotoing@insa-rennes.fr

Keywords: Thermo-Viscoplastic Model, Thermal Biaxial Tensile Test, Calibration

Abstract. In this study, an inverse identification strategy based on the finite element model updating (FEMU) method is proposed to calibrate the parameters of a temperature and strain rate dependent constitutive model. The mechanical responses of a dedicated cruciform specimen with heterogeneous temperature field under biaxial loading are employed to supply information to the inverse scheme. A combination of Particle Swarm Optimization (PSO) and SIMPLEX optimization algorithm is employed to find the optimal values of the material parameters. In order to validate the proposed identification strategy, a virtual experiment is designed and performed with a reference material constitutive model. The proposed strategy is proved to be feasible as all seven parameters of the constitutive model are accurately identified. In addition, the influences of measurement noise of force, temperature, and strain data are analyzed by means of a sensitivity study. The experimental data after the localized necking should be avoided for parameter identification. The proposed inverse identification strategy shows good robustness to strain noise.

Introduction

Advanced processes in engineering, such as hot stamping, high-speed metal forming or electrically-assisted manufacturing, involve complex mechanical behaviors and multi-axial loading conditions [1]. For a numerical analysis of these forming processes, it is necessary to construct the constitutive model that takes into account the thermo-visco-plastic hardening relations. Over the years, a number of phenomenological or physical constitutive models have been proposed to describe the temperature and strain rate dependent flow stress of sheet metals. Phenomenological models usually incorporate strain hardening models with temperature softening and strain rate hardening multiplicative or additive factors, such as Johnson-Cook model [2] or Khan-Huang-Liang model [3]. The physical-based models are usually based on the thermodynamics and kinetics of dislocations, such as Zerilli-Armstrong model [4] or Voyiadjis-Abed model [5]. In recent years, machine-learning approaches have also made significant progress in the phenomenological representation of the material macroscopic responses [6].

The constitutive models are strongly nonlinear and often involve many parameters to allow high fitting potential and flexibility. Therefore, strategies for the identification of model parameters are crucial. The conventional strategy relies on some conventional tests, such as the uniaxial tensile test or bulge test, to calibrate the parameters from analytical solutions based on the assumption of homogeneous stress distribution. However, in the case of high temperature and quasi-static forming, the necking strain of certain ductile materials can be at extremely low levels [7]. Necking introduces unreliability to the parameter identification since it breaks the assumption of homogeneous stress distribution. In addition, most of the sheet metals are deformed with a heterogeneous stress field in practical production. Adopting a conventional strategy may lead to an incomplete characterization of mechanical responses for the multi-axial loading conditions [8]. An inverse identification strategy based on full-field measurements is considered as a promising



alternative to overcome the drawbacks of conventional strategies [9, 10]. Avril et al. [11] presented a complete overview and comparison of five mainstream methods of this strategy. Among them, the FEMU is a very intuitive one, it can be applied to non-linear constitutive models and complex specimen shapes with heterogeneous stress fields. The principle of the FEMU is to minimize the gap between the numerical predictions and experimental measurements by iteratively updating the model parameters. The mapping relationship between the prediction and experiment can be established based on displacement, strain, force, etc. In addition, the minimization of the gap requires efficient and robust optimization algorithms, such as gradient-based algorithms (e.g., the Levenberg–Marquardt method) or metaheuristics (e.g., the genetic algorithms (GA) [12], particle swarm optimization (PSO) [13]).

For the FEMU method, the finite element (FE) model should reproduce the experiment as close as possible, including the specimen geometries, loadings, and boundary conditions. In addition, the mesh refinement of the FE model is also crucial, as it directly affects the precision and time consumption of the method. It should be noted that the computational cost is the main factor limiting the application of the FEMU method since the FE analysis is required at each iteration. Investigating the sensitivity of the FEMU method to the measurement noise is also essential. For complex experiments with heterogeneous strain and temperature fields, the full-field measurements obtained by the Digital Image Correlation (DIC) method or infrared cameras always contain data noise. Sensitivity studies allow the evaluation of possible biases in parameter identification caused by data noise.

In recent years, the combination of biaxial tensile testing with inverse identification strategies has shown great potential in characterizing the mechanical properties of metal sheets. Biaxial stretching is a special case of multi-axial loading. It can be used to identify anisotropic yield criterion parameters by achieving very heterogeneous strain and stress distributions through cruciform specimen design [14, 15], and also to determine the forming limits at various strain paths by adjusting the biaxial tensile ratios [16]. In addition, Liu et al. [17] employed a cruciform specimen and the FEMU method to identify the sheet metal hardening at large strains. The geometry of the specimen was carefully designed and the thickness reduction in the central zone permitted to reach a high level of homogeneous deformation under equi-biaxial tension. To the best of the authors' knowledge, studies combining biaxial tensile tests with inverse strategies to calibrate constitutive models that consider both temperature and rate effects are very unusual. Thus, the aim of this study is to conduct a feasibility study on the application of the FEMU method combined with biaxial tensile tests for the calibration of a thermo-viscoplastic constitutive model. A virtual experiment based on the thermal biaxial tensile test with a dedicated cruciform specimen [17] is designed and performed with a reference thermo-viscoplastic constitutive model in ABAQUS software. The advantage of the virtual experiment is that it can provide ideal full-field data for the parameters identification and the identified results can be directly validated by the reference model. This is very convenient for feasibility and sensitivity studies. In the following sections, the framework of FEMU and the details of the FE model are introduced. The effects of mesh size, plastic heat, and optimization algorithm are discussed. In addition, the robustness of the proposed inverse identification scheme is investigated by adding Gaussian noise to the force and strain data and considering the reconstruction errors of the temperature field.

Virtual biaxial tensile test

Reference thermo-viscoplastic constitutive model.

A Voce-type model [18] is used to define the temperature and strain rate-dependent plastic behavior of the virtual material with the following equations:

$$\bar{\sigma} = \sigma_0(T) + K_1 \exp(-K_2 T) \times \sqrt{1 - \exp[-K_3 \exp(K_4 T) \bar{\epsilon}_p]} \times \dot{\epsilon}^{m_0 \exp(m_1 T)} \quad (1)$$

$$\sigma_0(T) = \{1 - T/T_m \times \exp[K_0(1 - T_m/T)]\} \times \sigma_0(T_0) \quad (2)$$

where K_i and m_i are material parameters. K_1 defines the hardening potential of the material. The hardening potential decreases exponentially with increasing temperature, and this temperature softening effect is defined by K_2 . m_0 and m_1 define the hardening effect of strain rate on flow stresses and this effect is temperature dependent. K_3 and K_4 introduce the effect of temperature on strain hardening. T is the temperature and $T_m = 617^\circ\text{C}$ is the melting temperature. $\dot{\epsilon}$ is the strain rate. $\sigma_0(T)$ is the initial yield stress with consideration of temperature effect. The values of these parameters are presented in Table 1, and Fig. 1 illustrates the effect of temperature and strain rate on the flow stresses.

Table 1. Material parameters for the reference model.

Parameter	K_0	K_1 (MPa)	K_2 (1/°C)	K_3	K_4 (1/°C)	m_0	m_1 (1/°C)
Value	0.2295	334.2	0.00307	2.293	0.00633	0.00564	0.00811

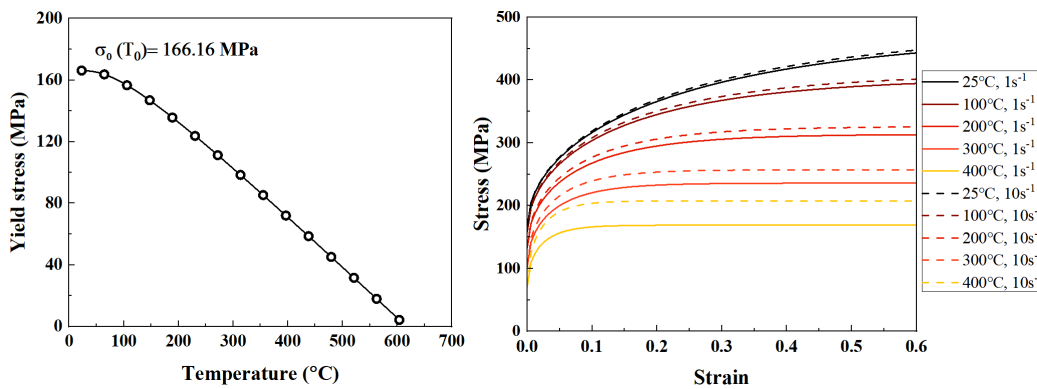


Fig. 1. Effect of temperature and strain rate on flow stresses.

FE model of the virtual biaxial tensile test

The virtual test is based on the thermal biaxial tensile test using induction heating method and employs the cruciform specimen proposed by Liu et al. [17]. The induction heating method has a faster heating rate compared to the conventional furnace heating method, and eliminates the space requirement of the furnace or insulated box and its limitation on the full-field measurements of the specimen. The heating principle works as follows: an induction coil heats a circular steel plate with a given power, and the plate heats the specimen through heat conduction and heat radiation. The top surface of the steel plate is just in contact with the specimen bottom surface and covers the specimen central area. Since an open local heating approach is adopted, the heat balance of the specimen is achieved by constant power induction heating and heat conduction to the air and grips, so the temperature distribution of specimen is non-uniform.

The virtual biaxial tensile test is modeled with the ABAQUS FE code and performed with the fully coupled temperature-displacement procedure. It consists of three stages: heating, thermal expansion, and thermal stretching. The material thermal properties (Young's modulus, Poisson's ratio, Thermal conductivity, etc.) used for the simulations are from [19], and the thermo-viscoplastic constitutive model is implemented in a UHARD subroutine. For the first stage, as shown in Fig. 2(a), the cruciform specimen is heated to the target temperature by the hot plate (in grey) positioned below the specimen and reaches thermal balance after a holding period. The plate is heated by setting a body heat flux in the central area to simulate a constant power heating situation. The bottom surface of the specimen is just in contact with the plate and the heating of the specimen is achieved by defining heat conduction and heat radiation properties between the specimen and the plate. In addition, to simulate the air heat transfer, an interaction of the surface film condition is defined to the surfaces of the specimen and plate; to simulate heat transfer in the grip regions of the specimen, surface film condition is also adopted but with a larger film coefficient. By adjusting the value of body heat flux, thermal balance can be reached in the specimen central area for different targeted temperatures (100°C, 200°C and 300°C). In the second stage, as shown in Fig. 2(b), a quarter of the specimen geometry is employed and thermal expansion of the specimen is simulated by introducing the historical temperature fields obtained from the heating stage. In the third stage, the specimens at different temperatures are equi-biaxial stretched at 0.02, 2, and 200 mm/s, respectively. For the velocity of 0.02 mm/s, the effect of plastic work on the specimen temperature is not considered. While, for the 2 and 200 mm/s cases, the simulation of the specimen temperature is based on the adiabatic condition assumption, i.e., without considering the heat transfer from the plate and air to the specimen. This is an omission of the thermal balance between the heating of the plate and the heat dissipation by the air in order to reduce the simulation time. To verify this, simulation results based on the assumption of adiabatic and isothermal conditions are compared at room temperature (RT, 23°C). The reason for choosing the RT condition is that the flow stress is higher at this temperature ensuing in a larger plastic work. As shown in Table 2, with 0.02 mm/s velocity and isothermal condition, the temperature of the specimen central element shows a slight increase. In the cases of 2 and 200 mm/s, the temperature increases significantly, but the temperatures obtained under adiabatic and isothermal conditions are approximately the same. The cruciform specimen is discretized through the eight-node brick solid elements with reduced integration (C3D8R). In order to balance simulation accuracy and computation time, mesh refinement with convergence check is performed for the specimen central area. As can be seen in Fig. 3, the equivalent strain of the specimen center element converges at a mesh size of 0.15 mm and the corresponding computation time is about 202 s (CPU processes: 8 cores, 2.2 GHz). In addition, three elements in the thickness direction are applied.

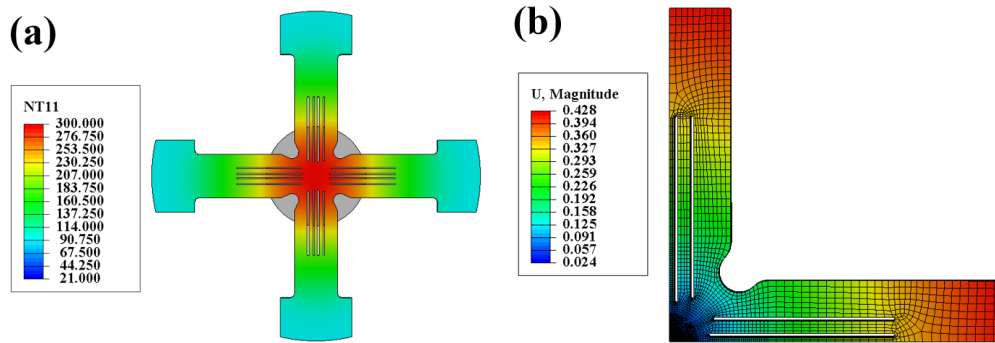


Fig. 2. (a) FE model with predicted temperature field for the heating stage (300°C), and (b) displacement field of the specimen after the thermal expansion.

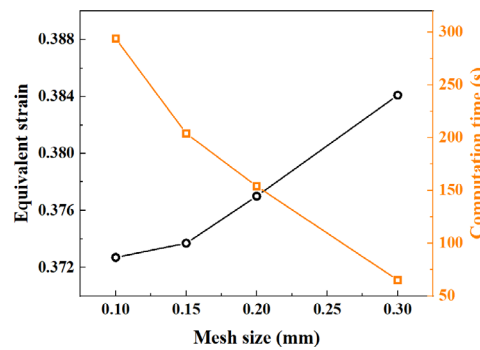


Fig. 3. Convergence analysis for the mesh refinement of the specimen central area.

Table 2. Temperature of the center element predicted based on the assumption of adiabatic and isothermal conditions.

0.02 mm/s	2 mm/s		200 mm/s	
Isothermal	Adiabatic	Isothermal	Adiabatic	Isothermal
23.1°C	39.8°C	39.7°C	54.9°C	55.4°C
(Strain 0.3)	(Strain 0.317)	(Strain 0.317)	(Strain 0.274)	(Strain 0.277)

In total, the virtual biaxial tensile tests under four temperatures (RT, 100°C, 200°C, 300°C) and three tensile velocities (0.02, 2, and 200 mm/s) are performed. Afterwards, the temperature fields of the specimens, the major and minor principal strains of the center element, and the force data of the two tensile axes are extracted. These data will be used for the inverse identification procedure.

Inverse Identification Procedure Based on FEMU Method

The flowchart of the FEMU method is shown in Fig. 4. The inverse identification procedure is divided into two steps: identification of parameters K_i followed by m_i . The other material parameters (Young's modulus, Poisson's ratio, Thermal conductivity, etc.) are kept the same as in the virtual experiment. Firstly, the temperature-dependent parameters (K_i) are identified under quasi-static loading (0.02 mm/s, corresponding to an average strain rate of 0.01 s^{-1}). Then, strain rate-dependent parameters (m_i) are identified for all the considered strain rate and temperature conditions. The FEMU method is achieved by using the mode-FRONTIER software platform allowing the coupling between the FE simulation code (ABAQUS software) and optimization

algorithms. The FE models of the third stage (in section 2) with the corresponding temperature fields are imported into the procedure, while the loadings on the two tensile axes are controlled by the virtual measured forces. The tensile forces are directly influenced by temperature and strain rate-dependent flow stresses. A cost-function is used to quantify the gap in the major and minor principal strains of the specimen center element between the simulation and the virtual experiment, which can be expressed as follow:

$$Q = \frac{1}{N_T + N_R} \sum_{T,R=1}^{N_T, N_R} Q_{N_T, N_R}(p) \tag{3}$$

$$Q_{N_T, N_R}(p) = \frac{1}{N_i} \sum_{i=1}^{N_i} \left\{ \sqrt{[\varepsilon_1^{sim}(i) - \varepsilon_1^{exp}(i)]^2 / [\varepsilon_1^{exp}(i)]^2} + \sqrt{[\varepsilon_2^{sim}(i) - \varepsilon_2^{exp}(i)]^2 / [\varepsilon_2^{exp}(i)]^2} \right\} \tag{4}$$

where p represents a set of material parameters. ε_1 and ε_2 are the major and minor principal strains, respectively. ε^{sim} and ε^{exp} are the principal strains obtained from simulation and virtual experiment, respectively. N_T is the number of temperature conditions, and N_R is the number of strain rate conditions. N_i is the total number of equally spaced time points defined in each simulation. The cost-function is calculated using a MATLAB script.

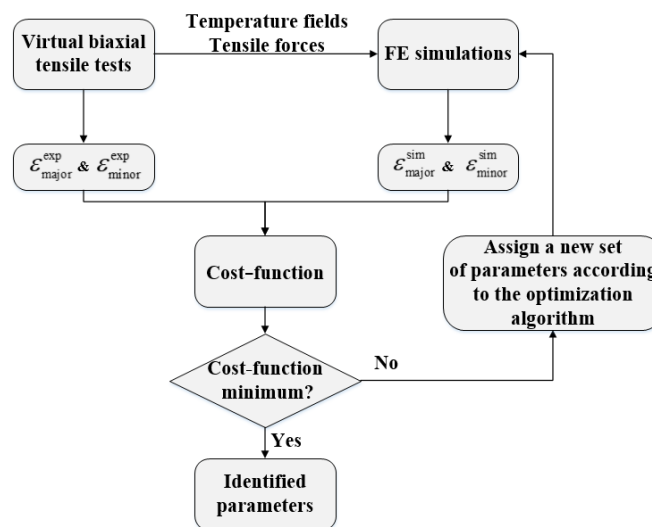


Fig. 4. Flowchart for the FEMU method.

The FEMU method minimizes the cost function by finding the optimal set of parameters, and the update iteration of the parameters is achieved by coupling an optimization method with the cost-function. In this work, a combination of PSO and SIMPLEX optimization algorithms is employed to identify the parameters K_i , while the parameters m_i are identified using only the SIMPLEX algorithm. The PSO consists of a swarm of potential solutions called particles [20]. These particles move through the search domain at a specified velocity to find the best solution. Each particle maintains a memory which helps it in keeping the track of its previous best position. In addition, the path of the particle also takes into account the global best position shared by the particle swarm. Since PSO does not use the gradient of the problem being optimized, it enables the parameters to be close to the global optimal position, but does not guarantee to find the exact value. Therefore, the SIMPLEX algorithm is employed to further determine the exact values of the parameters. For the parameters of PSO, the number of particles is 10, the inertia weight is 0.6, cognitive learning weight is 2, social learning weight is 0.5 and turbulence is 0.01. The Uniform

Latin Hypercube algorithm is adopted to define the initial set of parameters for each particle, which allows for a regular equally spaced over the parameter ranges. For the identification of K_i , 1400 iterations are performed using PSO and 266 iterations are performed by SIMPLEX. Table 3 lists the parameter ranges, the identified parameter values and the relative errors with respect to the reference values. It could be found that the PSO locates the approximate values of the parameters within a large parameter range. Based on this, the ranges of parameters are reduced and then the exact values of the parameters are obtained by the SIMPLEX. For the identification of parameters m_0 and m_1 , 12 FE simulations are required for each iterative cycle, which implies a huge computational time. Therefore, only the SIMPLEX algorithm is used for the identification of m_i , considering that it is an efficient algorithm with a fast convergence rate. For the identification of m_i , 60 iterations are performed. Overall, the relative errors of the identified parameters are at a low level, which proves the feasibility of the proposed inverse identification procedure.

Table 3. Identified parameters of the constitutive model.

Parameter	PSO			SIMPLEX		
	Range	Identified value	Error	Range	Identified value	Error
K_0 (MPa)	[0.1, 0.4]	0.252	9.9%	[0.2, 0.3]	0.2267	1.2%
K_1	[200, 400]	340.7	1.9%	[300, 350]	333.4	0.23%
Step 1 K_2 (1/°C)	[0.001, 0.005]	0.00316	2.9%	[0.002, 0.004]	0.00306	0.32%
K_3	[1, 5]	2.199	4.1%	[2, 4.5]	2.299	0.26%
K_4 (1/°C)	[0.001, 0.1]	0.00626	1.1%	[0.003, 0.008]	0.00633	0%
Step 2 m_0				[0.001, 0.009]	0.00544	3.5%
m_1 (1/°C)				[0.005, 0.01]	0.00821	1.2%

Sensitivity analysis

In Section 3, the parameters of the constitutive model are accurately identified based on the tensile forces, principal strains, and temperature fields obtained from the virtual tests. However, noises are inevitable when physical measurements are done. Therefore, in this section, the effects of measurement noises are evaluated. A comparison study is performed with and without noise using the simulation of thermal biaxial tensile test under a temperature of 300°C and a tensile velocity of 200 mm/s. White Gaussian noises are added to the tensile force data of the two tensile axes, and the disrupted force is given by $\tilde{F}(t) = F(t) + n(0, s)F_{max}$. Where $n(0, s)$ is a normal (Gaussian) distribution with zero mean and standard deviation s , F_{max} is the maximum value of the force. As shown in Fig. 5(a), two levels of noise ($s = 0.005$ and $s = 0.01$) are tested. The relative error of the principal strains between the simulations with and without noise is also shown in this figure. It can be found that the significant increase in the relative error occurs at the decrease of the tensile force, which usually means the occurrence of necking. While, during the uniform deformation stage, both levels of noise bring weak influence on the principal strains of the specimen center element. Therefore, identification using the test data before the occurrence of necking seems to be effective.

During the test, factors such as the offset of the heat source location and suboptimal contact can cause asymmetric distribution and shift of the specimen temperature field. Although the temperature field can be measured by an infrared thermal camera, the temperature field reconstruction in the FE simulation inevitably contains errors. To evaluate the influence of temperature field reconstruction errors, the center of the originally symmetrically distributed temperature field in the simulation is shifted so that the highest temperature is moved from the original center of the specimen to 5 mm off-center, and the temperature of the center point is

decreased from 300 °C to 290 °C. The tensile forces of the two tensile axes are then compared, and the results are shown in Fig. 5(b). It can be seen that the deviation of the force curve appears at the beginning of the necking stage. This indicates that the temperature field reproduced in the FE model should refer to the experimentally measured results and the data from the force decrease stage should be avoided for parameter identification.

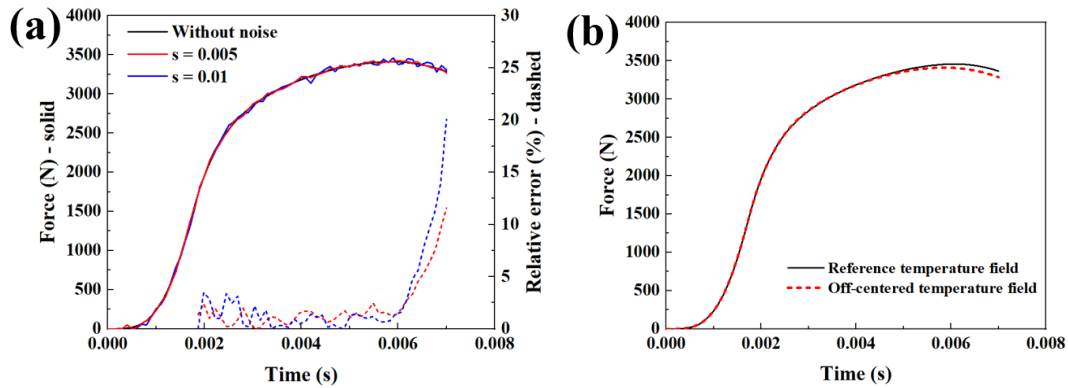


Fig. 5. (a) Tensile force (acquisition rate 10000Hz) with and without gaussian noise, and the relative error of the principal strains between the cases with and without noise. (b) Tensile force predicted with reference temperature field and off-centered temperature field.

In order to evaluate the effect of strain noise, white Gaussian noises ($n = 0, 0.1$) are added to the principal strain data, then the identification of parameters K_i is performed based on the procedure introduced in section 3. The identified values of K_i with the corresponding errors are given in Table 4, and a comparison between the flow stresses of reference model and the identified model is given in Fig. 6. The result indicates that K_0 exhibits a significant sensitivity to the strain noise. K_0 is the parameter that determines the temperature-dependent initial yield stress, so the principal strain data from the initial deformation stage are dominant for its identification. The added Gaussian noise is multiplied by the maximum value of strain, which makes the magnitude order of the noise excessive for the strain of the initial stage. This can be the reason for the large error in K_0 identification. From Fig. 6, the flow stress of the identification model is in good agreement with that of the reference model, therefore the proposed inverse identification process is considered to have good robustness to the strain noise.

Table 4. Identified parameters K_i based on the strain data with Gaussian noise.

Parameter	K_0	K_1 (MPa)	K_2 (1/°C)	K_3	K_4 (1/°C)
Identified value	0.2804	341.8	0.00323	2.196	0.00617
Error	22.1%	2.2%	5.2%	4.2%	2.5%

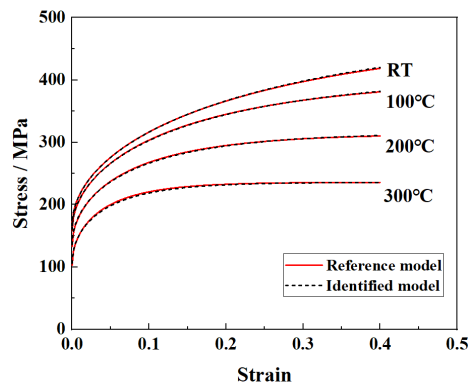


Fig. 6. Comparison of flow stresses between the reference model and the identified model.

Summary

In this work, the feasibility of the proposed inverse identification strategy for identifying the thermo-viscoplastic constitutive model is analyzed. A virtual biaxial tensile test is designed and used to supply information for the constitutive model parameters identification. The main conclusions are as follow:

- The proposed inverse identification strategy is based on the FEMU method with biaxial tensile test. The parameters K_i and m_i are accurately identified based on the force, temperature and strain data obtained from the virtual tests.
- The PSO algorithm is used to track the approximate values of the parameters and reduce the ranges of parameters, then the exact values of the parameters are obtained by the SIMPLEX algorithm.
- Sensitivity study shows that using force and temperature data before the occurrence of necking is preferable in order to reduce the effect of data noise. The identification of the parameter K_0 is sensitive to strain noise. The proposed inverse identification strategy exhibits a sufficient robustness to strain noise.

References

- [1] R. Zarea, J. Fernández-Sáez, An implicit consistent algorithm for the integration of thermoviscoplastic constitutive equations in adiabatic conditions and finite deformations, *Int. J. Solid. Struct.* 43 (2006) 1594-1612. <https://doi.org/10.1016/j.ijsolstr.2005.03.070>
- [2] G.R. Johnson, W.H. Cook, A constitutive model and data for metals subjected to large strains, high strain rates and high temperatures, In *Proceedings of the 7th International Symposium on Ballistics*, The Hague, The Netherlands, 19–21 April 1983, pp. 541-547.
- [3] A.S. Khan, Y.S. Suh, R. Kazmi, Quasi-static and dynamic loading responses and constitutive modeling of titanium alloys, *Int. J. Plast.* 20 (2004) 2233-2248. <https://doi.org/10.1016/j.ijplas.2003.06.005>
- [4] F.J. Zerilli, R.W. Armstrong, Dislocation-mechanics based constitutive relations for material dynamics calculations, *J. Appl. Phys.* 61 (1987) 1816-1825.
- [5] G.Z. Voyiadjis, F.H. Abed, Microstructural based models for bcc and fcc metals with temperature and strain rate dependency, *Mech. Mater.* 37 (2005) 355-378. <http://doi.org/10.1016/j.mechmat.2004.02.003>
- [6] X. Li, C.C. Roth, C. Bonatti, D. Mohr, Counterexample-trained neural network model of rate and temperature dependent hardening with dynamic strain aging, *Int. J. Plast.* 151 (2022) 103218. <https://doi.org/10.1016/j.ijplas.2022.103218>
- [7] H. Shang, P. Wu, Y. Lou, J. Wang, Q. Chen, Machine learning-based modeling of the coupling effect of strain rate and temperature on strain hardening for 5182-O aluminum alloy, *J. Mater. Process. Tech.* 302 (2022) 117501. <https://doi.org/10.1016/j.jmatprotec.2022.117501>
- [8] J.M.P. Martins, A. Andrade-Campos, S. Thuillier, Comparison of inverse identification strategies for constitutive mechanical models using full-field measurements, *Int. J. Mech. Sci.* 145 (2018) 330-345. <https://doi.org/10.1016/j.ijmecsci.2018.07.013>
- [9] Z. Wang, S. Zang, X. Chu, S. Zhang, L. Leotoing, Identification of 7B04 aluminum alloy anisotropy yield criteria with conventional test and Pottier test at elevated temperature, *Results. Phys.* 15 (2019) 102655. <https://doi.org/10.1016/j.rinp.2019.102655>
- [10] P. Prates, A. Pereira, N. Sakharova, M. Oliveira, J. Fernandes, Inverse strategies for identifying the parameters of constitutive laws of metal sheets, *Adv. Mater. Sci. Eng.* 2016 (2016) 1-18. <https://doi.org/10.1155/2016/4152963>

- [11] S. Avril, F. Pierron, Y. Pannier, R. Rotinat, Stress reconstruction and constitutive parameter identification in plane-stress elasto-plastic problems using surface measurements of deformation fields, *Exp. Mech.* 48 (2008) 403-419. <https://doi.org/10.1007/s11340-007-9084-2>
- [12] J.H. Holland, *Adaptation in natural and artificial systems: an introductory analysis with applications to biology, control, and artificial intelligence*, Ann. Arbor., MI, University of Michigan Press.
- [13] J. Kennedy, R.C. Eberhart, Particle Swarm Optimization, in: *Proceedings of the IEEE International Conference on Neural Networks*, Piscataway, vol. IV, 1995, pp. 1942-1948.
- [14] P.A. Prates, M.C. Oliveira, J.V. Fernandes, A new strategy for the simultaneous identification of constitutive laws parameters of metal sheets using a single test, *Comp. Mater. Sci.* 84 (2014) 102-120. <http://doi.org/10.13140/RG.2.2.25692.80004>
- [15] S. Zhang, L. Leotoing, D. Guines, S. Thuillier, S. Zang, Calibration of anisotropic yield criterion with conventional tests or biaxial test, *Int. J. Mech. Sci.* 85 (2014) 142-151. <https://doi.org/10.1016/j.ijmecsci.2014.05.020>
- [16] Z. Wang, D. Guines, X. Chu, L. Leotoing, Characterization of forming limits at fracture from shear to plane strain with a dedicated cruciform specimen, *Int. J. Mater. Form.* 7 (2022) 15. <http://doi.org/10.1007/s12289-022-01658-8>
- [17] W. Liu, D. Guines, L. Leotoing, E. Ragneau, Identification of sheet metal hardening for large strains with an in-plane biaxial tensile test and a dedicated cross specimen, *Int. J. Mech. Sci.* 101-102 (2015) 387-398. <https://doi.org/10.1016/j.ijmecsci.2015.08.022>
- [18] J. Liang, D. Guines, L. Leotoing, Effect of temperature and strain rate on the plastic anisotropic behavior characterized by a single biaxial tensile test, *Procedia Manuf.* 47 (2020) 1532-1539. <https://doi.org/10.1016/j.promfg.2020.04.346>
- [19] J. Gao, Y. Cao, L. Lu, Z. Hu, K. Wang, F. Guo, Y. Yan, Study on the interaction between nanosecond laser and 6061 aluminum alloy considering temperature dependence, *J. Alloy. Compd.* 892 (2022) 162044. <https://doi.org/10.1016/j.jallcom.2021.162044>
- [20] A.G. Gad, Particle Swarm Optimization Algorithm and Its Applications: A Systematic Review, *Arch. Computat. Meth. Eng.* 29 (2022) 2531-2561. <http://doi.org/10.1007/s11831-021-09694-4>